Sensors and Materials, Vol. 32, No. 3 (2020) 859–872
MYU Tokyo

S & M 2143

Prediction of Thermal Deformation of Rotary Table in Multifunction Machine Tool Using Neural Networks

Shao-Hsien Chen[1*] and Wun-Syuan Huang[2]

[1]The Graduate Institute of Precision Manufacturing, National Chin-Yi University of Technology, No.57, Sec. 2, Zhongshan Rd., Taiping Dist., Taichung 41170, Taiwan (R.O.C.)
[2]Department of Mechanical Engineering, National Chin-Yi University of Technology, No.57, Sec. 2, Zhongshan Rd., Taiping Dist., Taichung 41170, Taiwan (R.O.C.)

(Received January 18, 2019; accepted December 29, 2019)

Keywords: rotation table, temperature rise, thermal deformation, backpropagation of artificial neural network

The five-axis machining center and mill-turn lathe are some of the modern machining technologies widely used around the world. The spindle of the mill-turn lathe is the power source for cutting and milling. The spindle often spins at 2000 rpm or more for higher milling accuracy and efficiency. However, as the rotation speed increases, so does the temperature and, thus, the accuracy deteriorates and the number of errors increases. As a result, it is important to measure and predict the thermal deformation in the spindle of the mill-turn lathe. For this study, temperature was measured at various points on the spindle. The deformation was measured using a gantry-type main axis. The temperature increase and deformation measurements were analyzed, and the results were used for the prediction using the backpropagation of an artificial neural network. From this, the machining accuracy can be improved by refining the structure design or compensation. The largest temperature increase was found to be 8 °C. The maximum deformations were 0.026 mm for the *X*-axis, 0.004 mm for the *Y*-axis, and −0.069 mm for the *Z*-axis.

1. Introduction

Multifunction machine tools (mill-turn lathes) are extensively employed in work piece machining in, for example, aeronautics and car wheels. The increase in rotary table rpm to up to N = 2000–2500 rpm results in the increase in temperature and thermal deformation. The prediction and suppression of the temperature increase and thermal deformation of the rotary table are technically insufficient. A high-speed rotary table is used in mill-turn lathes for multi-axis machining and milling/cutting integrated machining. Current applications include the machining of aeronautic engine casing and aluminum alloy wheels in the automobile industry. The work pieces are mostly large, thin, and round or disclike. Therefore, the mill-turn machine provides a solution for one-stop machining in terms of simplification in the work piece process.

*Corresponding author: e-mail: e6036@ncut.edu.tw
https://doi.org/10.18494/SAM.2020.2598

ISSN 0914-4935

However, the faster the spin of the rotary table, the more accurate the cutting surface. The temperature of the spindle increases rapidly owing to the direct-drive motor, bearing, and rotational inertia. Still, the resulting temperature increase leads to deformation as the machine spins at a high speed. Therefore, maintaining the same accuracy while the machine spins at a high speed is the subject of this study.[1–3]

The study was intended to analyze and predict the thermal deformation in mill-turn machines. The high-speed rotation of the spindle has become inevitable for the machining of large and thin work pieces. When analyzing a *B*/*C* axis rotary table, the *C*-axis rotated at N = 2000 rpm. For the analysis and prediction of thermal deformation in a spindle, the *B*/*C* axis rotary table was mounted on a gantry-type workstation. A temperature sensor was attached to the spindle to measure the temperature rise of the spindle at a high rpm and the accuracy after the temperature rise. The effect of the temperature rise on the accuracy of the spindle was investigated. Then, the thermal deformation was predicted and analyzed using the backpropagation of an artificial neural network (BPN).

2. Theory and Principle of Temperature Rise

The rotary table of a mill-turn machine was selected as the subject of this study. As shown in the figure, the drive came from a direct-drive motor with the maximum rpm at N = 2000–2500 rpm to match the movements of the bearing and spindle. The increase in rotation speed will increase heat, and the more easily generated thermal deformation reduces the accuracy of the multi-axis machine tool application as shown in Fig. 1.

The analysis and prediction were performed on the rotary table for this study. The heat generation was proportional to rotation speed and moment. The equation shows that the moment is related to loading and lubrication. The change in temperature and the duration of the steady state were observed during the experimental analysis. The BPN was introduced for the prediction and analysis. In Eq. (1), the main explanation is that the heat generated by the bearing is proportional to the speed and frictional torque. The following is the heat generated in the mechanical system:[4,5]

$$Q = 1.047 \times 10^{-4}\, nM, \tag{1}$$

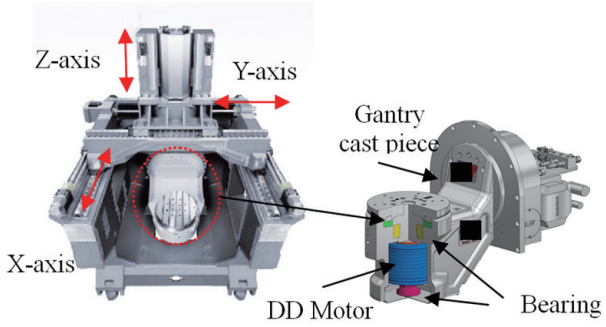

Fig. 1. (Color online) Workstation of a mill-turn machine.

where Q is the heat generated by the bearing, n is the bearing rpm, and M is the friction moment (Nm). In Eq. (1), M is the sum of the moment induced by the bearing loading (M_1) and that induced by the bearing lubricant (M_2). Therefore, the friction moment is expressed as

$$M = M_1 + M_2. \tag{2}$$

In Eq. (2), the moment induced by the bearing loading is

$$M_1 = \mu_0 f_0 \cdot F \cdot dm/2, \tag{3}$$

where μ_0 is the friction coefficient, f_0 is the direction coefficient of loading, F is the bearing loading (N), and dm is the nominal internal diameter of bearing (m). The moment induced by the bearing lubricant is

$$M_2 = f_1 \cdot (v \cdot n)^{2/3} dm^3, \tag{4}$$

where f_1 is the factor associated with the types of bearing structure and lubricant, v is the viscosity of the lubricant (m^2/s), dm is the nominal internal diameter of the bearing (m), and n is the bearing rotation speed (rpm).

From the above, it is clear that the higher the spindle rotation speed, the greater the heat generated by the bearing. More heat is generated as the spindle bearing operates for a long time, leading to temperature rise, thermal deformation, and in turn, compromised accuracy.[6–8]

The accuracy of machining centers is affected by static and drive errors. Bryan[9] suggested that the static error accounts for 35% of the effect on the machine accuracy. The static error comprises thermal deformation and geometric errors. Weck *et al.*[10] mentioned that 50% of the total error in a machine comes from those due to thermal expansion, indicating that heat has a considerable effect on machine accuracy.

When a machine is operating, the friction between parts, among other factors, generates heat. However, this heat affects the machine indirectly, through thermal conduction, radiation, and convection. The heat leads to a temperature rise in many parts of the machining center and, eventually, deformation due to thermal errors, as shown in Fig. 2. The result is the compromised accuracy of the machining center.[3,8,11]

3. Artificial Neural Network Analysis

3.1 Introduction to artificial neural network

The artificial neural network is essentially a computer system that mimics the human nerve system and is capable of learning, thinking, and problem solving. The artificial neural network simulates thermal deformation with a large quantity of simple artificial neurons and produces results using a simple computation. Therefore, its system or process can be described mathematically, as shown in Fig. 3. In 1989, Lippmann[12] pointed out that the BPN requires only one or two hidden layers to solve a problem of any form.[12,13]

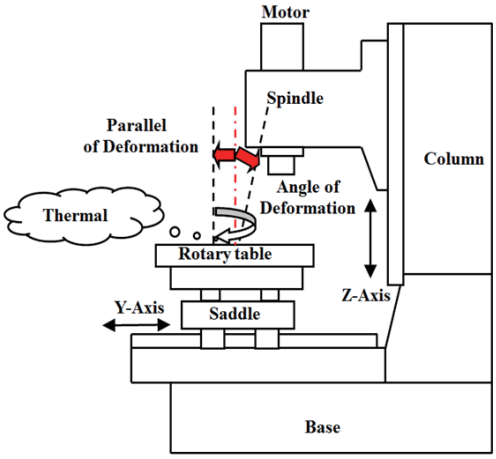

Fig. 2. (Color online) Machine tool thermal deformation diagram.

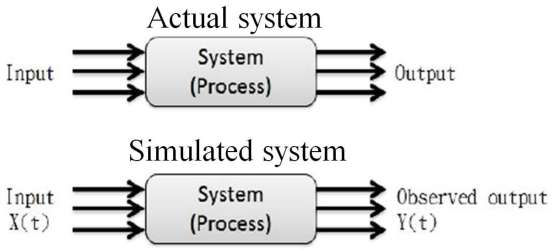

Fig. 3. Artificial neural network theory.

3.2 Algorithm of BPN

The artificial neural network mimics the data processing system of a biological neural network, which is a network nerve system consisting of 1011 nerve cells or neurons. Figure 4 shows an artificial neuron or processing unit. Every processing unit is capable of receiving one or more input signals and producing an output signal after a simple computation in the middle layer. The relationship between inputs and outputs is generally expressed using the weighted product and function of inputs.[14,15]

$$net_j = \sum_{i=1}^{n} W_{ij} X_i - \theta_j, \tag{5}$$

$$Y_j = f(net_j), \tag{6}$$

where net_j is the aggregation function, which is the weighted product of inputs minus bias, Y_j is the output signal, X_i is the input signal, θ_j is the threshold, f is the conversion coefficient, and W_{ij} is the neuron intensity, i.e., the weight.

The prediction was made using the BPN for this experiment. The basic architecture of the network consisted of an input layer, a hidden layer, and an output layer, which were connected with neurons, as shown in Fig. 5.

3.3 Transfer function

Also called the activation function, the transfer function is the most important processing tool in the artificial neuron network. It is a function that figures out the thresholds of biological neurons and works as a reflective rule that transforms the inputs of neurons to outputs according to the sum of weights. The use of different transfer functions makes the artificial neural

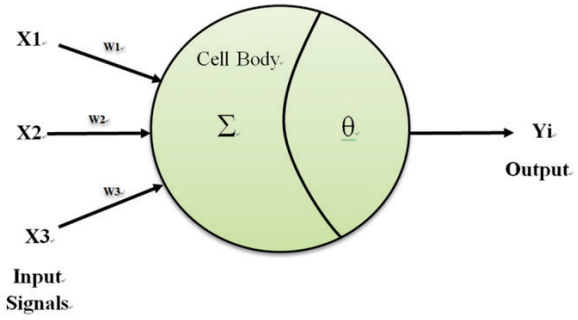

Fig. 4. (Color online) Artificial neuron model.

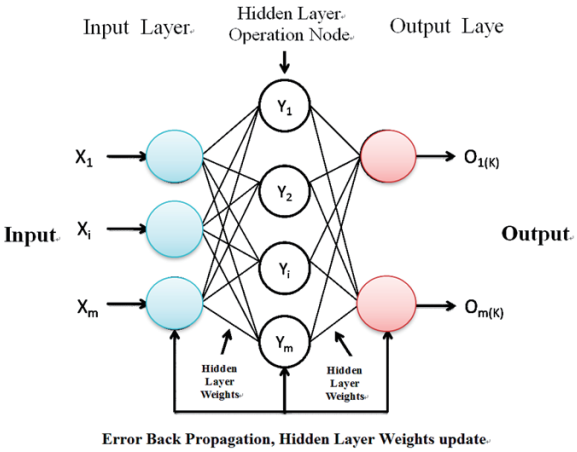

Fig. 5. (Color online) Architecture of the BPN.

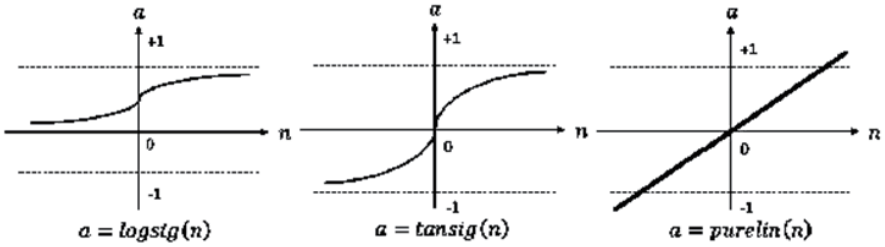

Fig. 6. Three transfer functions commonly used.

network model produce different changes. Figure 6 shows the most commonly used functions: (1) log-sigmoid transfer function, (2) hyperbolic tangent sigmoid function, and (3) linear transfer function. In this study, we use a hyperbolic tangent sigmoid function for analysis.[7]

3.4 Building BPN model

The BPN is extremely sensitive to the number of neurons in the hidden layer. Too many or too few neurons will affect the output result. It is necessary to determine how many neurons are required before making any prediction. Equations (7)–(9) were used in the calculations to respectively produce 4, 8, and 16 neurons, and, therefore, the setup and learning were made between 4 and 16 neurons. There were five input variables, namely, two bearing temperature points, two motor temperature points, and one at the cast piece of the spindle, in addition to time as the network input. The network outputs were the changes in thermal deformation for the *X*-, *Y*-, and *Z*-axes.

$$N_H = (N_I + N_O)/2, \tag{7}$$

$$N_H = N_I + N_O, \tag{8}$$

$$N_H = (N_I + N_O) \times 2, \tag{9}$$

where N_H is the number of neurons in the hidden layer, N_I is the number of neurons in the input layer, and N_O is the number of neurons in the output layer.

Equations (7)–(9) were used in the calculations for region 4–16 neurons, and then the correlation coefficient R was determined to optimize the input parameters after the training. The simulation distribution after the training is shown in Fig. 7. Table 1 shows the comparison between different numbers of neurons. The ratio of training values to verification values is 7:3, and the hyperbolic tangent sigmoid function is used in the transition. It is clear that 16 neurons produced the best R and distribution. The correlation coefficient R is given as

$$R = \sum_{t=1}^{N} (Q_t - \bar{Q}_t)(\hat{Q}_t - \bar{\hat{Q}}_t) / \sqrt{\sum_{t=1}^{N} (Q_t - \bar{Q}_t)^2 \times \sum_{t=1}^{N} (\bar{Q}_t - \bar{\hat{Q}}_t)^2}, \tag{10}$$

where N is the number of data, Q_t is the measured data, $\hat{Q}_t$ is the estimated data, $\bar{Q}_t$ is the measured average data, and $\bar{\hat{Q}}_t$ is the estimated average data.

4. Experimental Setup and Equipment

4.1 Experimental setup

This study consisted of two parts. The first part consisted the measurement and analysis of thermal deformation. For the purpose of the experiment, rpm was selected as the controllable factor, and the rotary table was set at the maximum rpm for testing. Therefore, the controllable factor was fixed. The measurement was focused on temperature. Temperature sensors were attached to the spindle bearing and motor for measurement to determine the temperature rise of the bearing. Secondly, for accuracy measurement, the test probe was mounted on the machining surface of the rotary table. The probe had to be aligned with the spindle within 0.002 mm. A displacement sensor was used to measure the thermal deformation of the entire machining surface of the rotary table. Figure 8 shows that the measurement equipment.

4.2 Experimental sequence and setup

The rotation speed was considered as the controllable factor at N = 2000–2500 rpm. As the temperature reached a steady state, the rotary table speed was decreased to N = 0 rpm

Table 1
Correlation coefficient R for different numbers of neurons.

No. of neurons	R for training	R for validation	R for test	All R
4	0.99984	0.99985	0.99985	0.99984
6	0.99984	0.99984	0.99983	0.99984
8	0.99988	0.99987	0.99988	0.99988
12	0.99991	0.99991	0.99989	0.99991
16	0.99992	0.99992	0.99991	0.99992

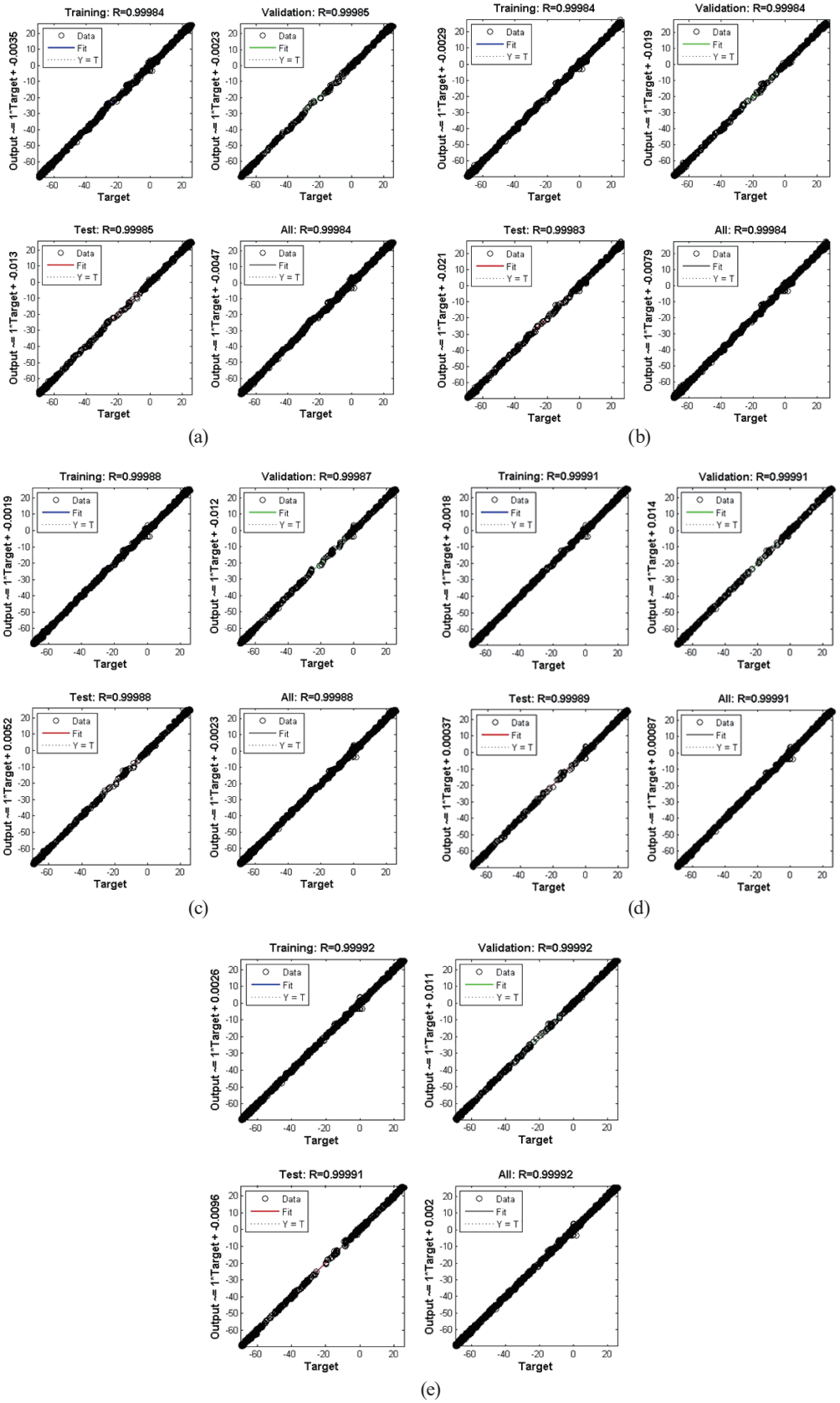

Fig. 7. (Color online) Simulation distribution after training. (a) Four, (b) six, (c) eight, (d) 12, and (e) 16 neurons.

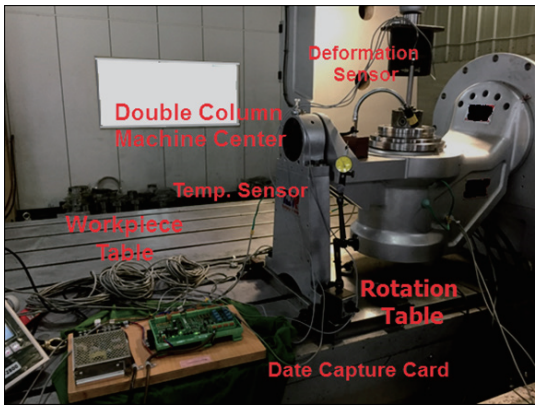

Fig. 8. (Color online) Measurement equipment and system for the thermal deformation of rotary table.

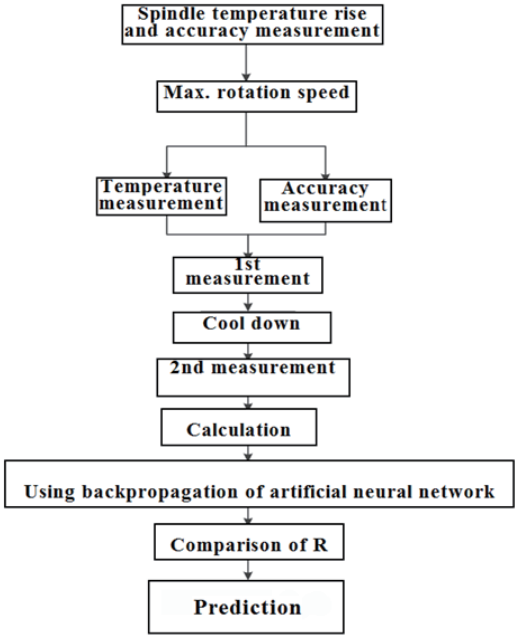

Fig. 9. Experimental flow and setup.

to return to the initial temperature. At this moment, the rotary table rpm was increased to N = 2000–2500 rpm. Again, the changes in temperature rise up to the steady state were observed. We determined whether the temperature rise and deformation were symmetric. The experimental sequence is shown in Fig. 9.

The temperature sensors were located at major hot spots, such as the bearing and motor, as shown in Fig. 10 and Table 2. They were located symmetrically for measurement and analysis. Seven sensors were mounted, including one that measured room temperature.

For the measurement of location accuracy, the test probe was fixed on the surface of the rotary table. Upon testing, the rotary table spun at a high rotation speed, resulting in thermal deformation. The displacement sensors were placed on each of the three axes (X, Y, and Z) of the gantry mill for measurement, as shown in Fig. 11. The displacement sensors on the X-, Y-, and Z-axes were fixed references. For this study, the thermal deformation measured from the rotary table was defined as negative (−) if the rotary table deformation caused the sensor to move toward the test probe as it started rotating and positive (+) if away from the probe.

An intelligent measurement module was used for temperature measurement in the experiment as shown in Fig. 10 in combination with IC-type temperature sensors. For accuracy measurement, the combination of an intelligent module and an eddy current displacement meter was used and mounted on the fixture designed for this experiment.

4.3 Mean square error (MSE) of estimation

For the prediction of the artificial neuron model and the BPN, how to select the proper number of neurons is very important. In this study, we use different numbers of neurons and

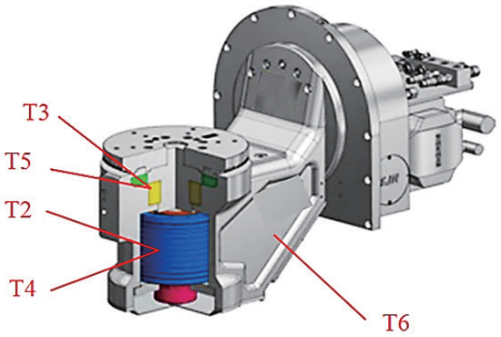

Fig. 10. (Color online) Locations of temperature sensors.

Table 2
Names and locations of temperature sensors.

Name	Location
T0	Room temperature
T1	Gantry cast piece
T2	Right side of motor
T3	Right side of bearing
T4	Left side of motor
T5	Left side of bearing
T6	Platform cast piece (machine temperature)

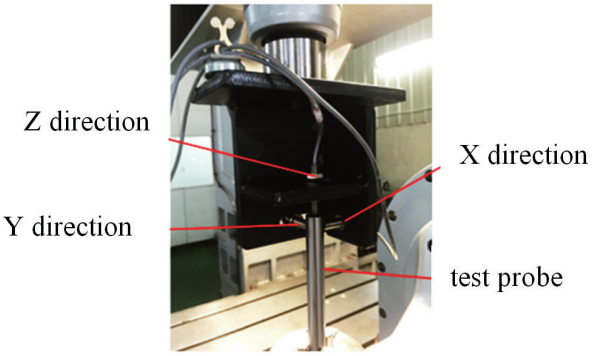

Fig. 11. (Color online) Actual placement of displacement sensors.

training times to find the most appropriate parameters with the mean square error and reduce the prediction error. The closer the MSE to 0, the smaller the error between the prediction value and the experimental value, as shown in Figs. 12(a)–12(c).

5. Results and Discussion

5.1 Effect of rotation speed on temperature rise

The temperature measurements taken during the experiment were collected and analyzed. As the spindle started to turn at the maximum rotation speed of N = 2500 rpm, the first experiment was conducted. The temperature was measured up to a steady state and the rotary table was allowed to cool, then the second experiment was conducted as soon as the temperature was close to room temperature. The two measurements were compared, as shown in Figs. 13 and 14 . It took 1 h and 10 min for the temperature to rise to a steady state for the first experiment and 1.5 h for the second experiment. Despite the difference in time to the steady state between the two experiments, the trends shown by the temperature rise curves were the same. The highest temperature rise occurred at the bearing for both experiments. For the first experiment, the temperature rise was as high as 8 °C, and for the second experiment, it was 5 °C. The motor, however, was water-cooled during the experiment. Therefore, the temperature

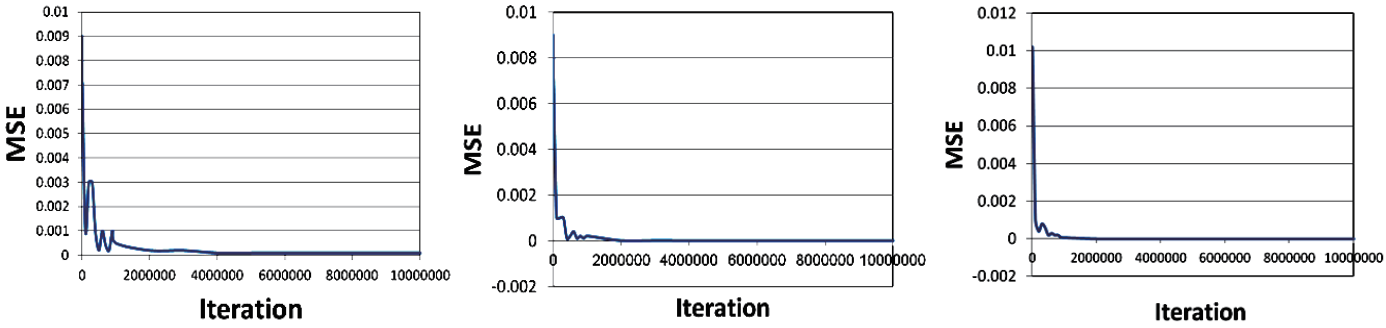

(a) (b) (c)

Fig.12. (Color online) MSEs of (a) four, (b) eight, and (c) 16 neurons.

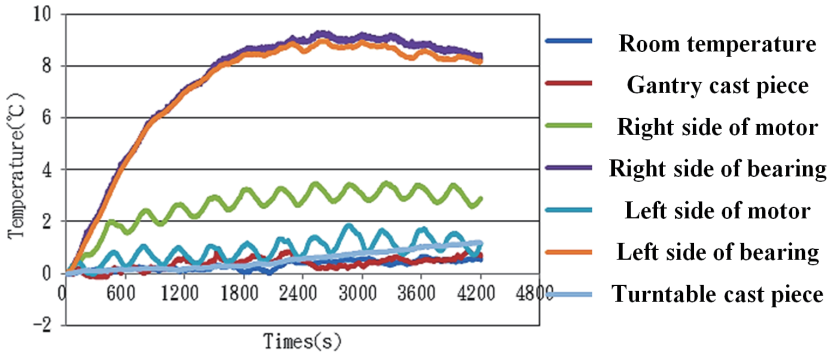

Fig. 13. (Color online) System temperature rise up to steady state in 1st experiment.

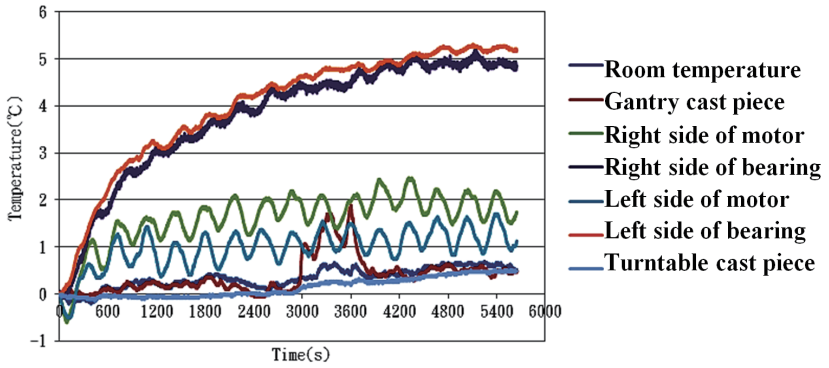

Fig. 14. (Color online) System temperature rise up to steady state in 2nd experiment.

rise on the right side of the motor was 2.8 °C for the first experiment and that on the left side was 1.1 °C. For the second experiment, the temperature rise was determined to be only 1.7 °C on the right side of the motor and 1.1 °C on the left side. On the temperature rise diagram, the temperature rise curves of the motor showed oscillation since the motor was cooled by the cooling machine.

5.2 Effect of temperature rise on accuracy

Displacement meters were used to measure the accuracy of the rotary table for the experiment. As the spindle started to turn at the maximum rotation speed of N = 2500 rpm, the thermal deformation generated during the rotations reduced the machining accuracy. The theory introduced above indicated that heat was generated as soon as the machining center started operating, and this heat caused the deformation of the rotary table and ultimately compromised the machining accuracy. The maximum rpm was selected as the control parameter for the experiment. When the spindle rotated, the temperature and displacement were measured simultaneously. The displacement measurement stopped as soon as the rotary table temperature reached a steady state. The second measurement of temperature rise and displacement started as the rotary table returned to its initial temperature. Again, the measurement stopped when the temperature reached a steady state, as shown in Figs. 15 and 16. The two measurements were compared to learn that, in the first experiment, the deformations were 0.026 mm for the X-axis, 0.004 mm for the Y-axis, and −0.069 mm for the Z-axis. The Y-axis deformation is relatively small as shown by the data, but the same cannot be said for the X- and Z-axes, which are the parts requiring improvement. In the second experiment, the deformations were 0.019 mm for the X-axis, −0.0046 mm for the Y-axis, and −0.028 mm for the Z-axis, indicating similar trends as the first. By comparing the deformation with the largest difference and the part with the largest temperature rise in the spindle, it was found that the bearing experienced a temperature rise of 8 °C in the first experiment and that of 5 °C in the second, indicating a difference of 3 °C. For the deformation, the Z-axis deformation was 2.5% greater in the first experiment than in the second, proving that the heat generated as the machining center operates has a profound effect on the deformation of the machining center, as shown in Table 3. This is what needs to be improved.

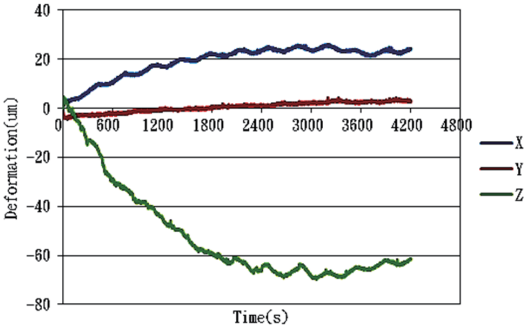

Fig. 15. (Color online) Deformation of the system in 1st experiment.

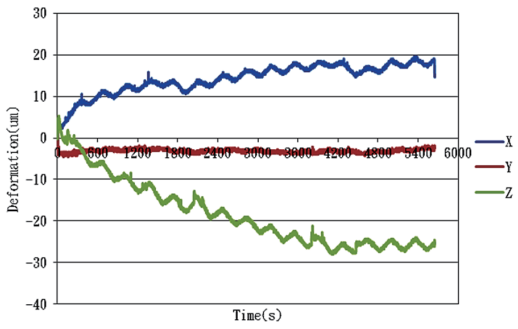

Fig. 16. (Color online) Deformation of the system in 2nd experiment.

Table 3
Highest temperature rise in spindle vs greatest deformation in each direction.

Deformation temp. rise	Bearing temp. rise of 8 °C in 1st experiment (mm)	Bearing temp. rise of 5.3 °C in 2nd experiment (mm)
X	0.026	0.019
Y	−0.0046	−0.0046
Z	−0.069	−0.028

5.3 Prediction of thermal deformation using BPN

When a rotary table starts to turn at a high rotation speed of N = 2000 rpm, the maximum application operating rotation speed is 80% of the designed maximum rotation speed, and it is easy to generate thermal deformation. On the other hand, the focus of this study was to determine whether the thermal deformation was symmetric and excessively large and, therefore, the BPN was employed for the prediction and analysis. The 16 neurons produced the best R and distribution, so 16 neurons were used for the prediction. With the artificial neural network optimized, the thermal deformation was predicted on the basis of the temperature rise and the time to steady state as the spindle rotated at the maximum rotation speed. The prediction result was the most accurate with 16 neurons, and in this study, we used the experimental template of the variation rate for the BPN prediction. The error ratios of the *X*-, *Y*-, and *Z*-directions are 9.6, 35, and 5.4%, respectively, as shown in Fig. 17.

The prediction and verification results use the mean absolute percentage error (MAPE) for analysis, the error ratios of the *x*-, *y*-, and *z*-directions are 0.0257, 0.0371, and 0.0183%, respectively. The error between the verification experiment and the prediction is very small, as shown in Fig. 18.

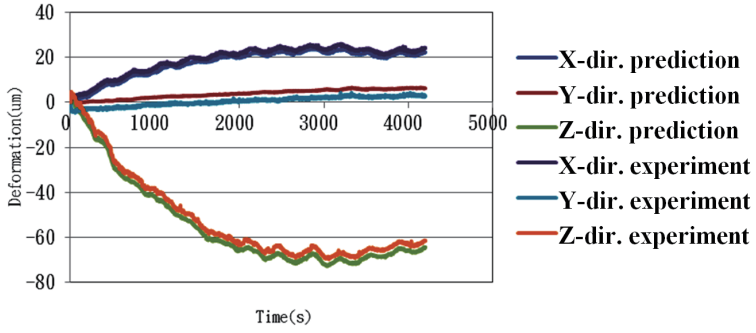

Fig. 17. (Color online) Prediction of thermal deformation at max. rotation speed of spindle with artificial neural network.

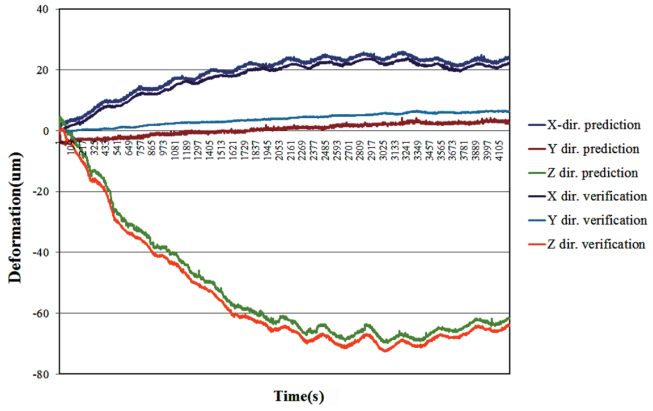

Fig. 18. (Color online) Verification experiment and BPN prediction diagram.

6. Conclusion

1. The rotary table is one of the many components of a machining center but plays a crucial role. From this experiment, we learned that the temperature rise of the rotary table itself has a significant effect on the deformation. To improve the machining accuracy, the temperature rise of the spindle is a factor to be considered.
2. The temperature rise diagrams show oscillation in the motor temperature. This is because the cooling machine used for the spindle was a traditional fixed-frequency ON/OFF cooling machine that operates to cool the spindle when the temperature is high. Such a method of cooling keeps the motor temperature fluctuating within a ±1 °C range as shown in the figures. That is why oscillation was found in the motor temperature rise, and this affects the accuracy. Also, in the deformation diagrams, there were some oscillations in the *X*- and *Z*-axis curves. This probably indicates the need to replace the cooling machine with one with a thermostat, as it will keep the spindle within the temperature range defined by the user and thus eliminate the oscillations in temperature and deformation and ultimately correct the deformation issue.
3. The room temperature was higher for the second experiment than for the first. However, the temperature after the steady state was lower than that after the first. A possible theory for this is that some of the parts on the spindle might become loose after a high rotation speed for a long period of time, which resulted in the lower temperature.

References

1 A. Błażejewski, W. Kwasny, J. Jedrzejewski, and T. Gim: J. Mach. Eng. **10** (2010) 26. https://www.researchgate.net/publication/260383841
2 Y.-C. Ye: Application and Implementation of Neural Network (Like Patterns, Taiwan, 1999).
3 Y.-C. Wang, M.-C. Kao, and C.-P. Chang: Measurement **44** (2011) 1183. https://www.researchgate.net/publication/251542218
4 Y.-L. Tsai: A Study of CNC Machine-tool Temperature Variation Measurement and Compensation Using Regression Analysis Method, Master's thesis, National ChinYi University of Technology (2012).
5 H.-Z. Yang: Mach. Mon. **24** (1998) 266.
6 G.-R. Zhang: J. Mach. Des. **324** (2010) 54.
7 Y.-T. Chang: Master's thesis, National ChinYi University of Technology (2014) (in Chinese). https://hdl.handle.net/11296/6jw32y
8 M. Gebhardt, J. Mayr, N. Furrer, T. Widmer, S. Weikert, and W. Knapp: CIRP Annals **63** (2014) 509. https://doi.org/10.1016/j.cirp.2014.03.029
9 J. Bryan: CIRP Ann. **39** (1990) 645. https://doi.org/10.1016/S0007-8506(07)63001-7
10 M. Weck, P. McKeown, R. Bonse, and U. Herbst: CIRP Ann. **44** (1995) 589. https://doi.org/10.1016/S0007-8506(07)60506-X
11 K. Liu, F. Chen, T. Zhu, Y. Wu, and M. Sun: Adv. Mech. Engin. **8** (2016) 1. https://doi.org/10.1177/1687814016657733
12 R. P. Lippmann: IEEE Commun. Mag. **27** (1989) 47. https://doi.org/10.1109/35.41401
13 J.-F. Mas and J.-J. Flores: J. Rem. Sen. **29** (2008) 617. https://doi.org/10.1080/01431160701352154
14 M. S. Nasr, M. A. E. Moustafa, H. A. E. Seif, and G. E. Kobrosy: Alexandria Eng. J. **51** (2012) 37. https://doi.org/10.1016/j.aej.2012.07.005
15 L. P. C. Verbeke, F. M. B. Vancoillie, and R. R. De wulf: Int. J. R. Sens. **25** (2004) 2747. https://doi.org/10.1080/01431160310001652385

About the Authors

Shao-Hsien Chen received his B.S. degree from National Chin-Yi University of Technology, Taiwan, in 1992 and his M.S. and Ph.D. degrees from National Chung Cheng University, Taiwan, in 2001 and 2006, respectively. From 2005 to 2009, he was an R&D manager at Ching Hung Machinery & Electric Industrial Co. LTD and AWEA Machinery & Electric Industrial Co. LTD, Taiwan. Since 2009, he has been an assistant professor at National Chin-Yi University of Technology. His research is a smart machine tool design and superalloy machining. (e6036@ncut.edu.tw)

Wun-Syuan Huang received her B.S. degree from Ming Hsin University of Science and Technology, Taiwan, in 2015 and her M.S. degree from National Chin-Yi University of Technology, Taiwan, in 2017. From 2017 to 2019, she was an engineer at Precision Machinery Research & Development Center, Taiwan. Her research is an smart machine and machine tool design.